Local-stability analysis of a low-dissipation heat engine working at maximum power output

I. Reyes-Ramírez[*]
Instituto Politécnico Nacional-UPIITA, Av. IPN 2580, Ciudad de México 07340, México

J. Gonzalez-Ayala
Departamento de Física Aplicada, Facultad de Ciencias, Universidad de Salamanca, 37008 Salamanca, Spain

A. Calvo Hernández
Departamento de Física Aplicada, Facultad de Ciencias
and Instituto Universitario de Física Fundamental y Matemáticas (IUFFyM), Universidad de Salamanca, 37008 Salamanca, Spain

M. Santillán[†]
Centro de Investigación y Estudios Avanzados del IPN Unidad Monterrey, Vía del Conocimiento 201, Parque PIIT, 66600 Apodaca NL, Mexico

(Received 9 August 2017; published 16 October 2017)

In this paper we address the stability of a low-dissipation (LD) heat engine (HE) under maximum power conditions. The LD system dynamics are analyzed in terms of the contact times between the engine and the external heat reservoirs, which determine the amount of heat exchanged by the system. We study two different scenarios that secure the existence of a single stable steady state. In these scenarios, contact times dynamics are governed by restitutive forces that are linear functions of either the heat amounts exchanged per cycle, or the corresponding heat fluxes. In the first case, according to our results, preferably locating the system irreversibility sources at the hot-reservoir coupling improves the system stability and increases its efficiency. On the other hand, reducing the thermal gradient increases the system efficiency but deteriorates its stability properties, because the restitutive forces are smaller. Additionally, it is possible to compare the relaxation times with the total cycle time and obtain some constraints upon the system dynamics. In the second case, where the restitutive forces are assumed to be linear functions of the heat fluxes, we find that although the partial contact time presents a locally stable stationary value, the total cycle time does not; instead, there exists an infinite collection of steady values located in the neighborhood of the fixed point, along a one-dimensional manifold. Finally, the role of dissipation asymmetries on the efficiency, the stability, and the ratio of the total cycle time to the relaxation time is emphasized.

DOI: 10.1103/PhysRevE.96.042128

I. INTRODUCTION

Since its appearance in 1975, in the seminal work of Curzon and Ahlborn (CA) [1,2], the Carnot-like endoreversible heat-engine model has been extensively studied. Extensions to address different heat transfer laws, operation regimes, and further modifications, have also been incorporated, yielding more realistic models with a good qualitative description of real-life devices. In addition to the optimization of operation regimes, an interesting question has to do with the capability of these systems to return to an stationary state after experiencing a perturbation. In 2001, Santillán *et al.* [3] introduced the local-stability analysis of endoreversible heat engines. Since then, the stability of different types of endoreversible engines has been studied. Not only their performance in a variety of operating regimes has been tackled [4–8], but also economic improvements have been discussed [9–11]. The stability of heat pumps, refrigerators, and generalized heat engines has been analyzed as well [8,12–21], complementing other possibilities, all of them within the endoreversible framework. Additionally, global stability has been analyzed in a few cases [22,23], in which conditions for global asymptotic stability were found. An important point to note in all these works is the use of a Carnot-like heat device models [1], with heat conduction laws explicitly defined in terms of temperature differences and appropriate conductances to account for the coupling of the working fluid with the external baths.

A significant conceptual development in the field of finite-time analysis of heat devices is the so-called low-dissipation model; originally introduced by Esposito *et al.* [24] for heat engines, and later extended by De Tomás *et al.* for refrigerator engines [25]. This model is a departure from a baseline Carnot cycle that considers the existence of dissipations along the isothermal processes. These dissipations are assumed to be proportional to some dissipative coefficients that enclose the intrinsic properties of the device, and are inversely proportional to the time duration of the corresponding isothermal processes. LD models usually regard the adiabatic processes as instantaneous [24–26]. However, models in which the time of adiabatic processes are taken into account have also been developed [27]. In all cases, the reversible regime is recovered in the limit of infinite contact times. In fact, the dissipative term makes the original LD model similar to the finite-time Brownian heat-engine model proposed by Schmiedl and Seifert in the optimal driving limit [28], and also equivalent to the minimally nonlinear irreversible heat engine, as demonstrated by Izumida

[*]ireyesram@hotmail.com
[†]msantillan@cinvestav.mx

and Okuda in Ref. [29]. An important feature of LD models is the possibility of obtaining upper and lower bounds for the efficiency at maximum power without any information regarding the specific-heat transfer mechanism. These limits are obtained by constraining the asymmetry of the dissipative coefficients. Additionally, in the symmetric dissipation case, the Curzon-Ahlborn efficiency, $\eta_{CA} = 1 - \sqrt{\tau}$ is recovered, with $\tau \equiv T_c/T_h$ being the cold-to-hot bath temperature ratio [2].

The extension of the local-stability-analysis framework of CA-like to LD models is not trivial. In all these kinds of models, some physical parameters are controlled in order to optimize the system performance. Examples of control parameters include working bath temperatures and contact times with external temperature reservoirs. However, in real life the values of control parameters are oftentimes indirectly regulated by design parameters such as system size, conductivity of thermal resistors, heat capacity of thermal baths, shape of potential energy landscapes, etc. In this regard, Santillán *et al.* [3] showed that the intermediate working bath temperatures of a Curzon-Ahlborn-Novikov engine (i.e., the parameters controlling the engine operation regime) are regulated by design parameters via an ordinary differential equations (ODE) system accounting for heat-flux balance. Furthermore, the engine optimal working temperatures are stable stationary solutions of the referred ODE system. Since intermediate working temperatures are not defined in the low-dissipation model proposed by Esposito *et al.* [24] due to the lack of any heat transfer laws, we assume in this work that a similar argument can be used for low-dissipation models regarding the contact times with heat reservoirs. That is, the system control parameters (contact times with heat reservoirs) are dynamic variables governed via a dynamic system by design parameters. We further expect that this dynamic system has a single stable stationary state, corresponding to the control parameter values that optimize the performance of the low-dissipation model. In summary, design parameter values would determine the steady value of control parameters (and so the system thermodynamic performance characteristics), as well as the stability of this stationary state. Thus, an interesting question is to investigate the correlation between stationary thermodynamic features and their dynamic stability.

To further justify the assumption that the contact times with heat reservoirs (whose sum equals the engine period) can be regarded as dynamic variables controlled by design parameters, we refer the reader to a specific example, namely, the β-type Stirling engine model introduced by Reséndiz-Antonio and Santillán [30]. This is a detailed model that considers in a simple way all the thermodynamic and mechanic details of such an engine, and serves as a basis to study the engine performance. In particular Reséndiz-Antonio and Santillán were able to demonstrate that the engine period is a dynamic variable that has a single stable steady state, and that the period stationary value and stability are determined by design parameters such as bath temperature ratio, thermodynamic characteristics of the working substance, moment of inertia of the fly wheel, friction coefficient, etc. The demonstration is based on the work-energy theorem:

$$K_{i+1} + K_i = W - f_i,$$

where K_i denotes the flywheel kinetic energy during the ith cycle, W is the engine thermodynamic work per cycle, and f_i represents energy loss due to friction during the ith cycle. Clearly, a stationary period is reached when $W = f_i$. Furthermore, this steady state is stable because if the engine period is too short (long), and thus the engine speed exceeds (is below) its corresponding stationary value, then the energy loss due to friction would be larger (smaller) than the engine work, and the kinetic energy would decrease in the next cycle, increasing (decreasing) the duration of the following period.

The objective of the present work is to study the stability properties of a LD engine, as well as the influence of dissipation symmetry (or asymmetry) on the system relaxation times and efficiency, in the maximum power regime, which is obtained from by optimizing the contact times with external heat baths [24]. The effects of dissipation asymmetry on the system entropy production, efficiency, and power output have been studied in Ref. [31], offering different scenarios regarding possible advantages that dissipation asymmetries may offer when switching from one operation regime to another [31]. In the present work we show that dissipation asymmetries may also play a relevant role in the stability of these kind of devices, and discuss how this could be an important aspect to consider, along with energetic characteristics, for a suitable design of heat devices. Finally, we study the relation between the system relaxation and total cycle times, and discuss its relevance.

The paper is organized as follows. In Sec. II we summarize the power-output optimization of Esposito's LD heat-engine model [24]. In Sec. III we present the stability analysis of an LD engine when the contact-time restitutive forces depend on the amounts of exchanged heat. In Sec. IV we present the stability analysis of an LD heat engine when the contact-time restitutive forces depend on heat fluxes. Finally, in Sec. V we present some concluding remarks.

II. MAXIMUM POWER IN LOW-DISSIPATION SCHEME

The starting point of the LD model [24] is a Carnot engine whose cycling period is very long to guarantee reversible operation conditions. Under these considerations, the system entropy changes due to the heat amounts exchanged with the hot (Q_h) and cold (Q_c) reservoirs are given by $\Delta S = Q_h/T_h$ and $-\Delta S = Q_c/T_c$, where T_h and T_c are the hot and cold reservoir temperatures, respectively. Next, a finite-time cycle in which the system has been taken away from reversible operation (see Fig. 1) is considered. If t_h and t_c, respectively, denote the contact times with the hot and cold reservoirs, the above relations become:

$$Q_h = T_h \Delta S \left(1 - \frac{\Sigma_h}{\Delta S t_h}\right),$$
$$Q_c = T_c \Delta S \left(-1 - \frac{\Sigma_c}{\Delta S t_c}\right). \quad (1)$$

In these last expressions ΔS is the engine quasistatic entropy change during the hot isothermal process [29], while Σ_h and Σ_c are the dissipative coefficients for isothermal processes at T_h and T_c, respectively. Since adiabatic processes are assumed to be instantaneous, the power output of this

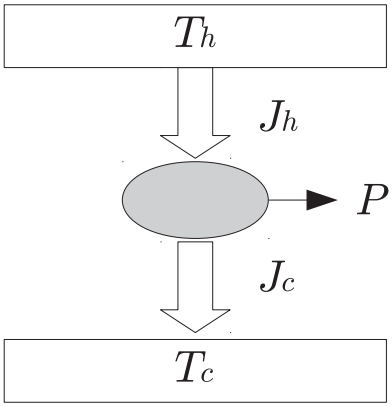

FIG. 1. Scheme of a low-dissipation heat engine.

engine is

$$P = \frac{-W}{t_c + t_h} = \frac{Q_h + Q_c}{t_c + t_h}. \tag{2}$$

In this scheme, the natural optimization parameters are t_h and t_c. The contact times corresponding to the maximum power output regime are

$$t_h^* = \frac{2\Sigma_h}{\Delta S(1-\tau)}(1+\sqrt{\tau\Sigma}),$$
$$t_c^* = \frac{2\tau\Sigma\Sigma_h}{\Delta S(1-\tau)}\left(1+\sqrt{\frac{1}{\tau\Sigma}}\right), \tag{3}$$

where $\Sigma \equiv \Sigma_c/\Sigma_h$ and $\tau = T_c/T_h$. Notice that these two expressions are monotonically increasing functions of the temperature ratio τ.

From Eqs. (1) and (3) the efficiency at maximum power, η_{MP}, is

$$\eta_{MP} = \frac{(1-\tau)(1+\sqrt{\tau\Sigma})}{(1+\sqrt{\Sigma})^2 + \tau(1-\Sigma)}, \tag{4}$$

which is a monotonically decreasing function of Σ, with lower and upper bounds given by

$$\frac{\eta_C}{2} \leqslant \eta_{MP} \leqslant \frac{\eta_C}{2-\eta_C}. \tag{5}$$

These lower and upper bounds are correspondingly reached in the limits $\Sigma \to \infty$ and $\Sigma \to 0$. In the symmetric case: $\Sigma = 1$ ($\Sigma_c = \Sigma_h$), the well-known CA efficiency η_{CA} is recovered.

III. STABILITY ANALYSIS BASED ON THE HEAT AMOUNTS EXCHANGED PER CYCLE WITH THERMAL BATHS

As previously discussed, since heat exchange mechanisms are not explicitly considered in the LD formalism, writing down the differential equations that govern the engine variables' dynamics is impossible without further assumptions. Hence, we propose that the contact times t_h and t_c are not constant but dynamic variables, whose stability is ensured by proper generalized restitutive forces. We suppose that if the contact time with one of the thermal baths is too long (short) during a cycle, then the corresponding heat exchange would be larger (smaller) than the stationary value. Thus, the stability of the steady state of t_h and t_c would be guaranteed if they are subject to restitutive forces that are functions of the corresponding heat exchanges or heat fluxes. In this section we explore the former case, and the latter case is addressed in Sec. IV.

From Eqs. (1), we rewrite the heat exchanges per cycle as follows:

$$Q_c = -T_h\tau\Delta S\left(1+\frac{\Sigma_h\Sigma}{\Delta S t_c}\right), \tag{6}$$
$$Q_h = T_h\Delta S\left(1-\frac{\Sigma_h}{\Delta S t_h}\right). \tag{7}$$

We define the following normalized (dimensionless) variables, which take into account the relative size of the dissipative terms with respect to the baseline reversible situation:

$$\widetilde{t_c} = \frac{\Delta S}{\Sigma_h}t_c,\ \widetilde{t_h} = \frac{\Delta S}{\Sigma_h}t_h,\ \widetilde{Q}_c = \frac{Q_c}{T_h\Delta S},\ \widetilde{Q}_h = \frac{Q_h}{T_h\Delta S}. \tag{8}$$

From the above definitions, Eqs. (6) and (7) become:

$$\widetilde{Q}_c = -\tau\left(1+\frac{\Sigma}{\widetilde{t_c}}\right), \tag{9}$$
$$\widetilde{Q}_h = \left(1-\frac{1}{\widetilde{t_h}}\right). \tag{10}$$

The normalized contact times at maximum power conditions are

$$\widetilde{t_c}^* = \frac{2\tau\Sigma}{1-\tau}\left(1+\frac{1}{\sqrt{\tau\Sigma}}\right), \tag{11}$$
$$\widetilde{t_h}^* = \frac{2}{1-\tau}(1+\sqrt{\tau\Sigma}). \tag{12}$$

We propose that the dynamics of $\tilde{t_c}$ and $\tilde{t_h}$ are governed by an ordinary differential equation (ODE) system of the form:

$$\frac{d\widetilde{t_c}}{dt} = f(\widetilde{Q}_c(\widetilde{t_c},\widetilde{t_h})), \tag{13}$$
$$\frac{d\widetilde{t_h}}{dt} = g(\widetilde{Q}_h(\widetilde{t_c},\widetilde{t_h})). \tag{14}$$

In order to guarantee the stability of the stationary contact-time values, f and g must be monotonically decreasing functions that satisfy: $f(\widetilde{Q}_c(\widetilde{t_c}^*,\widetilde{t_h}^*)) = g(\widetilde{Q}_h(\widetilde{t_c}^*,\widetilde{t_h}^*)) = 0$. The simplest way to achieve these requirements is by assuming that the dynamic system governing the dynamics of $\widetilde{t_c}$ and $\widetilde{t_h}$ is as follows:

$$\frac{d\widetilde{t_c}}{dt} = A(\widetilde{Q}_c(\widetilde{t_c}^*,\widetilde{t_h}^*) - \widetilde{Q}_c(\widetilde{t_c},\widetilde{t_h})), \tag{15}$$
$$\frac{d\widetilde{t_h}}{dt} = B(\widetilde{Q}_h(\widetilde{t_c}^*,\widetilde{t_h}^*) - \widetilde{Q}_h(\widetilde{t_c},\widetilde{t_h})), \tag{16}$$

with A and B constant.

From the way it was constructed, the dynamical system in Eqs. (15) and (16) has a single steady state given by $t_c = \widetilde{t_c}^*$ and $t_h = \widetilde{t_h}^*$. As it is well known, the local stability of this steady state is determined by the eigenvalues and eigenvectors

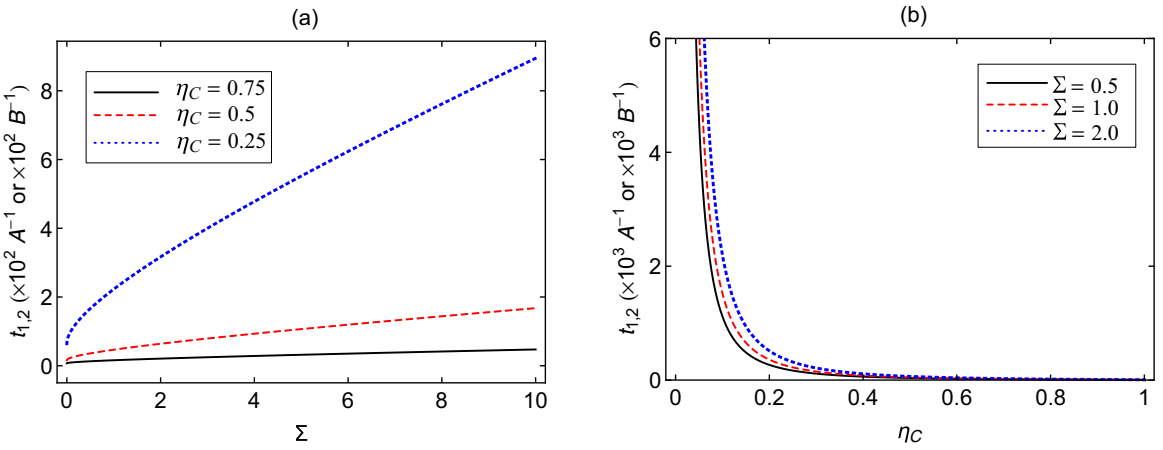

FIG. 2. (a) Plot of relaxation times versus Σ for three different values of ηC (see Eqs. (28) and (29)). (b) Plot of relaxation times versus ηC for different values of Σ.

of the corresponding Jacobian matrix [32]:

$$\mathcal{J} = -\begin{bmatrix} A\frac{\partial \widetilde{\dot{Q}}_c}{\partial \tilde{t}_c}\big|_{\tilde{t}_c^*,\tilde{t}_h^*} & A\frac{\partial \widetilde{\dot{Q}}_c}{\partial \tilde{t}_h}\big|_{\tilde{t}_c^*,\tilde{t}_h^*} \\ B\frac{\partial \widetilde{\dot{Q}}_h}{\partial \tilde{t}_c}\big|_{\tilde{t}_c^*,\tilde{t}_h^*} & B\frac{\partial \widetilde{\dot{Q}}_h}{\partial \tilde{t}_h}\big|_{\tilde{t}_c^*,\tilde{t}_h^*} \end{bmatrix}. \tag{17}$$

It is straightforward to prove after some algebra that the resulting matrix is

$$\mathcal{J} = -\begin{bmatrix} -A\xi(\tau,\Sigma) & 0 \\ 0 & -B\xi(\tau,\Sigma) \end{bmatrix}, \tag{18}$$

where

$$\xi(\tau,\Sigma) = \left(\frac{1-\tau}{2(\sqrt{\Sigma\tau}+1)}\right)^2. \tag{19}$$

Given that $\mathcal{J}$ is diagonal, its eigenvalues are simply

$$\lambda_1 = -A\xi(\tau,\Sigma), \quad \lambda_2 = -B\xi(\tau,\Sigma). \tag{20}$$

Furthermore, since $\xi(\tau,\Sigma)$ is a positive definite function, both λ_1 and λ_2 are real and negative. This means, on one hand, that the system steady state is stable, but this is not surprising because it follows from the proposed dynamical system for $\tilde{t}_c$ and $\tilde{t}_h$ [Eqs. (15) and (16)]. On the other hand, it is possible to define relaxation times as

$$t_{1,2} \equiv -\frac{1}{\lambda_{1,2}}, \tag{21}$$

which provide useful insights on the system-stability strength. It follows after a little algebra that

$$t_1 = A^{-1}\left(\frac{2(\sqrt{\Sigma\tau}+1)}{1-\tau}\right)^2, \tag{22}$$

$$t_2 = B^{-1}\left(\frac{2(\sqrt{\Sigma\tau}+1)}{1-\tau}\right)^2. \tag{23}$$

In the limit of infinite thermal gradients between the thermal reservoirs, that is $\tau \to 0$, the relaxation times tend to the following values,

$$t_1(\tau\to 0) = \frac{4}{A}, \quad t_2(\tau\to 0) = \frac{4}{B}, \tag{24}$$

which are independent of the symmetry or asymmetry of the dissipative coefficients. Meanwhile, when there is thermal equilibrium between heat reservoirs ($\tau = 1$),

$$\lim_{\tau\to 1} t_{1,2} \to \infty. \tag{25}$$

This happens because no restitutive force can bring back the system to the steady state due to thermal equilibrium. For any other value of τ, both relaxation times are monotonically increasing functions of Σ. Thus, they reach their lower bound in the limit where all dissipations are produced while the system is in contact with the hot reservoir ($\Sigma \to 0$):

$$t_1(\Sigma=0) = \frac{4}{A(1-\tau)^2}, \quad t_2(\Sigma=0) = \frac{4}{B(1-\tau)^2}. \tag{26}$$

In the opposite situation, when dissipations occur mostly while the system is in contact with the cold reservoir, both relaxation times diverge:

$$\lim_{\Sigma\to\infty} t_{1,2} \to \infty. \tag{27}$$

The steady-state relaxation times can also be written in terms of $\eta_C = 1-\tau$ and Σ:

$$t_1 = A^{-1}\left(\frac{2(\sqrt{\Sigma(1-\eta_C)}+1)}{\eta_C}\right)^2, \tag{28}$$

$$t_2 = B^{-1}\left(\frac{2(\sqrt{\Sigma(1-\eta_C)}+1)}{\eta_C}\right)^2. \tag{29}$$

According to Eqs. (28) and (29), the limit values for t_1 and t_2 are

$$\lim_{\eta_C\to 0} t_{1,2} = \infty, \quad t_1(\eta_C=1) = \frac{4}{A}, \quad t_2(\eta_C=1) = \frac{4}{B}, \tag{30}$$

and

$$t_1(\Sigma=0) = \frac{4}{A\eta_C^2}, \quad t_2(\Sigma=0) = \frac{4}{B\eta_C^2}, \quad \lim_{\Sigma\to\infty} t_{1,2} = \infty. \tag{31}$$

The dependence of the relaxation times on Σ and η_C is illustrated in Fig. 2. Observe that $t_{1,2}$ are respectively inversely proportional to A and B. This is an expected behavior from the dynamic equations (15) and (16). As a matter of fact, parameters A and B should have information regarding the

system design, size, etc. However, given the generality of low-dissipation models, this is not apparent. Notice as well that both relaxation times are monotonically decreasing functions of η_C. This implies that the larger the thermal gradient between the external reservoirs, the stronger the steady-state stability. This behavior is contrary to that described in the original paper on the stability of a Curzon-Ahlborn engine [3]. Evidently, this means that the formalism here proposed for the LD-model dynamics is not equivalent to that imposed by the heat-conducting laws onto the Curzon-Ahlborn model. Nonetheless, further work is necessary to fully understand this discrepancy. The relaxation-time dependence on Σ is also interesting. It basically states that Σ must be made as small as possible in order to enhance the engine stability. When contrasted with the result in Ref. [24] regarding the system efficiency:

$$\frac{\eta_C}{2} = \lim_{\Sigma\to\infty} \eta < \lim_{\Sigma\to 0} \eta = \frac{\eta_C}{2-\eta_C}. \tag{32}$$

We can see that decreasing the entropy production along the cold part of the cycle (i.e., decreasing Σ) not only enhances the system stability but also increases its efficiency, a desirable property while designing heat devices.

Heat engines commonly perform a cyclic processes in a continuous way. Thus, it is desirable that the system returns to the steady state within a cycle period. This can be used as a constraint for coefficients A and B. From Eqs. (11) and (12), the total cycle time at maximum power is

$$\tilde{t}^*_{\rm tot} = \tilde{t}^*_c + \tilde{t}^*_h = \frac{2}{\eta_C}(1+\sqrt{(1-\eta_C)\Sigma})^2. \tag{33}$$

On the other hand, from Eqs. (22) and (23), the total relaxation time is

$$\begin{aligned} t_{\rm relax} &= t_1 + t_2 \\ &= \frac{2}{\eta_C}(1+\sqrt{(1-\eta_C)\Sigma})^2 2\left(\frac{A^{-1}+B^{-1}}{\eta_C}\right) \\ &= 2\left(\frac{A^{-1}+B^{-1}}{\eta_C}\right)\tilde{t}^*_{\rm tot}. \end{aligned} \tag{34}$$

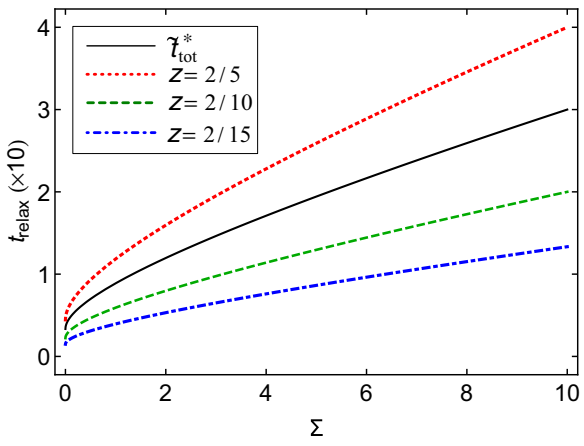

FIG. 3. Comparison of three relaxation times with the total cycle time at the maximum power steady state. For this plot we have used $\tau = 2/5$, in order to fulfill the requirement in Eq. (35) $z = A^{-1} + B^{-1} < 3/10$.

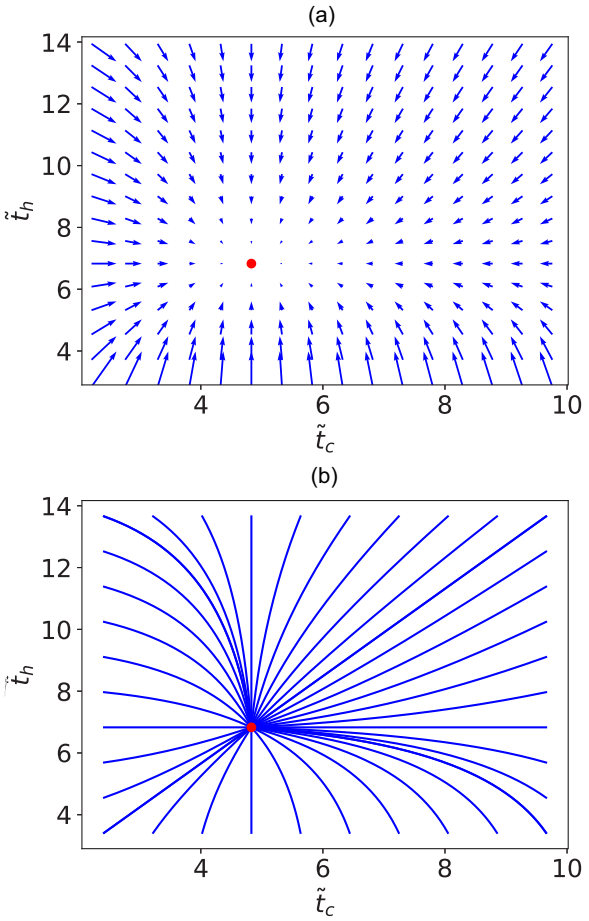

FIG. 4. (a) Quiver plot of the velocity vector field given by the ODE system in (15)–(16), and (b) phase-space trajectories computed by numerically solving the same equations. The parameter values used for these plots are: $A = B = 1$, $\Sigma = 1$, and $\tau = 0.5$. The system fixed point corresponding to these parameter values is represented with a red dot.

Hence, in order to have $\tilde{t}^*_{\rm tot} > t_{\rm relax}$, A and B must fulfill the following relation:

$$A^{-1} + B^{-1} < \frac{\eta_C}{2} \leqslant \frac{1}{2}. \tag{35}$$

A comparison of cycle and relaxation times in different scenarios can be appreciated in Fig. 3. There, we can see two different cases where the condition in Eq. (35) is fulfilled and one case where it is not. As $z \equiv A^{-1} + B^{-1}$ diminishes, the difference between the relaxation time and the characteristic total operation time is more noticeable. Also, as dissipations due to contact with the cold reservoir become more relevant ($\Sigma \gg 1$), the difference between both times is more pronounced. As mentioned before, we found that decreasing the value of Σ improves the system efficiency and stability, but also increases the relaxation times (making them closer to the cycle time), which might not be a desirable property.

All previous analyses are strictly valid in an infinitesimal neighborhood around the steady state. To test whether our results can be extended further, we numerically explored the system behavior by varying initial conditions. In Fig. 4

we show the velocity vector field of the ODE system in (15)–(16), plotted as a quiver plot on the corresponding phase space, as well as numerically computed phase-space trajectories. Although these plots correspond to specific values of parameters A, B, Σ, and τ, their qualitative characteristics maintain when such parameter values are changed. Observe that the system fixed point is globally stable, thus extending the results of the former local stability analysis.

IV. STABILITY ANALYSIS BASED ON THE HEAT FLUXES FROM THERMAL BATHS

In this section we study an equivalent description of the LD model, in which the optimization variables are the characteristic total time and the partial contact time with the cold reservoir. To this end, we introduce the following set of dimensionless variables [33]:

$$\widetilde{\Sigma}_c = \Sigma_c/\Sigma_T, \quad \alpha \equiv t_c/(t_c+t_h), \quad \widetilde{t} = \frac{\Delta S}{\Sigma_T}(t_c+t_h), \tag{36}$$

with $\Sigma_T = \Sigma_h + \Sigma_c$. In terms of these variables, the corresponding dimensionless heat fluxes are given by

$$\dot{\widetilde{Q}}_c \equiv \frac{Q_c}{\widetilde{t}T_c\Delta S} = -\left(1+\frac{\widetilde{\Sigma}_c}{\alpha\widetilde{t}}\right)\frac{1}{\widetilde{t}}, \tag{37}$$

$$\dot{\widetilde{Q}}_h \equiv \frac{Q_h}{\widetilde{t}T_c\Delta S} = \left(1-\frac{1-\widetilde{\Sigma}_c}{(1-\alpha)\widetilde{t}}\right)\frac{1}{\tau\widetilde{t}}, \tag{38}$$

while the dimensionless power output is

$$\widetilde{P} = \dot{\widetilde{Q}}_c + \dot{\widetilde{Q}}_h. \tag{39}$$

In this case the values of the variable that maximize $\widetilde{P}$ are [33]

$$\alpha^* = \frac{1}{1+\sqrt{\frac{1-\widetilde{\Sigma}_c}{\tau\widetilde{\Sigma}_c}}}, \tag{40}$$

$$\widetilde{t}^* = \frac{2}{1-\tau}(\sqrt{\tau\widetilde{\Sigma}_c}+\sqrt{1-\widetilde{\Sigma}_c})^2. \tag{41}$$

Gonzalez-Ayala *et al.* [34] have shown that this set of optimal states can yield efficiency-power curves similar to those arising from Curzon-Ahlborn-like endoreversible heat engines, and from irreversible heat engines, depending on the time constraints imposed on the system. Open parabolic curves are obtained when the partial contact time is fixed to $\alpha = \alpha^*$, while closed looped curves are achieved when the total time is constrained to $\widetilde{t} = \widetilde{t}^*$.

To develop a dynamical system for this normalization scheme we assumed that the system dynamic variables are α and $\widetilde{t}$, and that the corresponding restitutive forces are functions of $\dot{\widetilde{Q}}_c$ and $\widetilde{P}$, respectively. The reason for this is that, $\widetilde{t}$ being the total cycle time, it is reasonable to assume that its dynamics depend on the engine power output, rather than on the partial heat fluxes. Following the development in the previous section we propose an ODE system given by:

$$\frac{d\alpha}{dt} = C(\dot{\widetilde{Q}}_c(\alpha^*,\widetilde{t}^*) - \dot{\widetilde{Q}}_c(\alpha,\widetilde{t})), \tag{42}$$

$$\frac{d\widetilde{t}}{dt} = D(\widetilde{P}(\alpha^*,\widetilde{t}^*) - \widetilde{P}(\alpha,\widetilde{t})), \tag{43}$$

with C and D constant. The local stability of the above-given steady state is determined by the following Jacobian matrix [32]:

$$\mathcal{J} = -\begin{bmatrix} C\frac{\partial\dot{\widetilde{Q}}_c}{\partial\alpha}\Big|_{\alpha^*,\widetilde{t}^*} & C\frac{\partial\dot{\widetilde{Q}}_c}{\partial\widetilde{t}}\Big|_{\alpha^*,\widetilde{t}^*} \\ D\frac{\partial\widetilde{P}}{\partial\alpha}\Big|_{\alpha^*,\widetilde{t}^*} & D\frac{\partial\widetilde{P}}{\partial\widetilde{t}}\Big|_{\alpha^*,\widetilde{t}^*} \end{bmatrix}. \tag{44}$$

After performing the corresponding algebra, this matrix becomes

$$\mathcal{J} = -\begin{bmatrix} C\frac{\partial\dot{\widetilde{Q}}_c}{\partial\alpha}\Big|_{\alpha^*,\widetilde{t}^*} & C\frac{\partial\dot{\widetilde{Q}}_c}{\partial\widetilde{t}}\Big|_{\alpha^*,\widetilde{t}^*} \\ 0 & 0 \end{bmatrix}. \tag{45}$$

Observe that $\mathcal{J}$ has a null row. This happens because, in the maximum power regime,

$$\frac{\partial\widetilde{P}}{\partial\alpha}\Big|_{\alpha^*,\widetilde{t}^*} = \frac{\partial\widetilde{P}}{\partial\widetilde{t}}\Big|_{\alpha^*,\widetilde{t}^*} = 0.$$

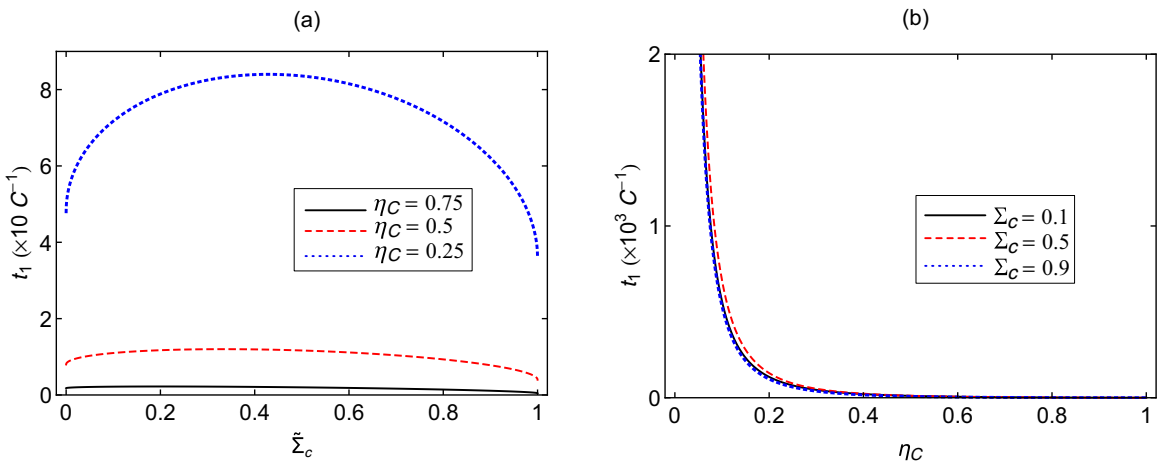

FIG. 5. (a) Plot of relaxation times versus $\widetilde{\Sigma}_c$ for three different values of η_C. (b) Plot of relaxation times versus η_C for three different values of $\widetilde{\Sigma}_c$.

The above result further implies that the linearized dynamical system becomes

$$\frac{d\alpha}{dt} = C\frac{\partial\tilde{\tilde{Q}}_c}{\partial\alpha}\bigg|_{\alpha^*,\tilde{t}^*}\alpha + C\frac{\partial\tilde{\tilde{Q}}_c}{\partial\tilde{t}}\bigg|_{\alpha^*,\tilde{t}^*}\tilde{t}, \tag{46}$$

$$\frac{d\tilde{t}}{dt} = 0, \tag{47}$$

and thus, $\tilde{t}$ is constant for any perturbation, while the general solution for α is of the form $\alpha(t) = c_1 e^{\lambda_1 t} + c_2 e^{\lambda_2 t}$. On the other hand, due to the fact that the determinant of $\mathcal{J}$ is zero, one of the eigenvalues equals zero, while the other is given by

$$\lambda = C\frac{\partial\tilde{\tilde{Q}}_c}{\partial\alpha}\bigg|_{\alpha^*,\tilde{t}^*}.$$

From this, a relaxation time for α can be defined as

$$t_1 = \frac{4(1-\eta_C)(1-\tilde{\Sigma}_c)(1+\sqrt{(1-\eta_C)\Sigma})^2}{\eta_C^2\, C}, \tag{48}$$

where Σ is as defined in Sec. III ($\Sigma \equiv \Sigma_c/\Sigma_h$). In Fig. 5, t_1 relaxation time is plotted as a function of $\tilde{\Sigma}_c$ and η_C. By imposing the condition that the relaxation time must be smaller than the total cycle time given by Eq. (41), we can constraint the possible values of C to

$$C > \frac{2(1-\eta_C)}{\eta_C}. \tag{49}$$

The fact that one of the Jacobian eigenvalues is zero further means that the system steady state is not isolated, but there is an infinite set of fixed point. Nevertheless, of all such fixed points, only $\alpha^*,\tilde{t}^*$ corresponds to the maximum power state.

To test to what extent the results above can be extended beyond an infinitesimal neighborhood around the steady state, we numerically explored the system dynamic behavior under numerous different initial conditions. In Fig. 6 we show a quiver plot for the velocity vector field corresponding the ODE system in (42)–(43), together with the corresponding numerically computed phase-space trajectories. Although these plots were computed with a specific set of parameter values, their qualitative characteristics remain unaltered when the parameter values are modified. There, we can see that only a small subset of initial conditions lead to trajectories (blue lines) that converge to the neighborhood of the steady state. From all other initial conditions, the trajectories converge to the $\dot{\alpha} = 0$ nullcline, and then they slowly diverge to $\alpha \to 0$ and $\tilde{t} \to \infty$ along this nullcline. This means that the engine eventually stops cycling and remains in contact with the hot thermal bath.

In Ref. [34], Gonzalez-Anaya *et al.* studied the role of time constraints in obtaining closed and open power-vs.-efficiency curves in the LD model. They found that constraining $\alpha = \alpha^*$ leads to open parabolic curves such as those of Carnot-like heat engine models with no heat leak. Interestingly, in all previous dynamic studies of endoreversible heat engines without heat leaks, the obtained steady states have been found to be stable. On the other hand, by imposing a fixed total operation time $\tilde{t} = \tilde{t}^*$ one obtains closed looped curves similar to those resulting from the introduction of a heat leak. The existence of a heat leak fixes the engine time arrow because the total entropy generation is positive ($\Delta S_{\text{Total}} > 0$), and means that the reversible limit is no longer achievable (indeed, the system becomes more irreversible as $\tilde{t}$ decreases). In view of the present discussion, our results imply that, when the total cycle time is perturbed (by means of heat-leak variations, for example), the system studied in the present section would not be able to spontaneously return to its original operation regime, and it may stop cycling altogether.

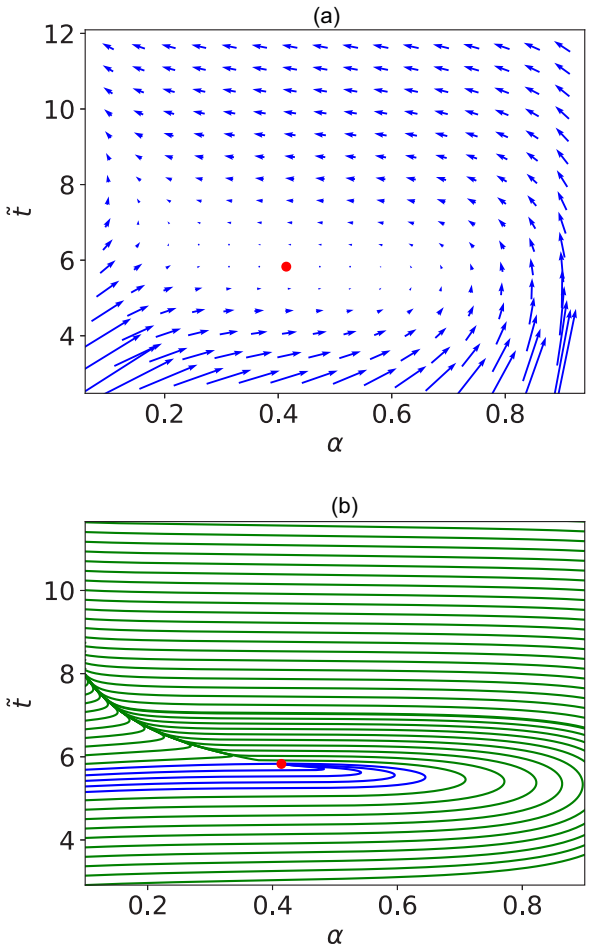

FIG. 6. (a) Quiver plot of the velocity vector field given by the ODE system in (42)–(43), and (b) numerically computed phase-space trajectories for the same ODE system. The parameter values used for these plots are: $C = D = 1$, and $\tilde{\Sigma}_c = \tau = 0.5$. The system fixed point corresponding to these parameter values is represented with a red dot. In (b), the trajectories converging to the neighborhood of the steady state are plotted in blue, while all other trajectories (which eventually diverge to $\alpha = 0$ and $\tilde{t} \to \infty$) are plotted in green.

V. CONCLUDING REMARKS

We have addressed the stability of a low-dissipation system operating at maximum power output. To this end, we considered two equivalent descriptions: one where the optimization variables are the contact time with the hot and cold reservoirs, and a second one where the optimization variables are the partial contact time with the cold reservoir and the total cycle time. In both cases the optimization variables

are regarded as dynamic variables, governed by restitutive forces. In the former case, the restitutive forces are assumed to linearly depend on the amount of exchanged heat, while in the latter case they are assumed to linearly depend on the heat fluxes.

When t_c and t_h are the dynamic variables, and the proposed restitutive forces are functions of the corresponding amount of exchanged heat per cycle (see Sec. III), it was possible to find a stable state and characterize the system stability in terms of its design characteristics: η_C and the dissipation ratio Σ (that measures dissipation symmetry or asymmetry). Furthermore, if dissipation mainly occurs while the engine is in contact with the hot reservoir, both the efficiency and the system stability are improved. Interestingly, this dissipation asymmetry has shown to be relevant for the system energetics (entropy production, efficiency, power output) and also plays an important role while switching operations regimes. On the other hand, when α and $\widetilde{t}$ are the dynamic variables, we found that α has a locally stable steady-state value, but $\widetilde{t}$ has not. Coincidentally, there is evidence suggesting that fixing the total cycle time is equivalent (within the context of Carnot-like engines) to introducing a heat leak into the system. To our understanding, this suggests that the fixating the engine cycle time would involve certain external control over the device, which would affect the system irreversibility through the total entropy generated per cycle, ΔS_{total}, and so altering these control mechanisms would irreversibly affect the cycle time. By considering the relaxation times and comparing them with the total cycle time one can impose some constraints over the dynamics of the system in order for the stability to be relevant when continuous cycling processes are carried out.

We finally note that the low-dissipation model is related with several physical systems, ranging from overdamped Brownian heat engines [28,35,36] to two-level quantum systems [37]. The extension of the macroscopic analysis here presented to these mesoscopic and/or quantum systems could be a further step in order to a better understanding of the role played by the fluctuations and probability distributions, not only for a particular operation regime but also of the device as a heat engine. The cases of power constraints such as in Refs. [38–42] or for stochastic heat engines at maximum efficiency [43] (to mention a few) might offer suitable applications on the road toward the understanding the dynamical control and stability analysis for low-dissipation heat devices.

ACKNOWLEDGMENTS

I.R.-R. acknowledges financial support from EDI-IPN-MÉXICO and COFAA-IPN-MÉXICO. M.S. acknowledges financial support from Cinvestav-MÉXICO. J.G.-A. acknowledges financial support from CONACyT-MÉXICO. A.C.H. acknowledges partial financial support from the Ministerio de Economía y Competitividad (MINECO) of Spain under Grant No. ENE2013-40644-R.

[1] F. Curzon and B. Ahlborn, Am. J. Phys. **43**, 22 (1975).
[2] A. Vaudrey, F. Lanzetta, M. Feidt, H. B. Reitlinger and the origins of the Efficiency at Maximum Power formula for Heat Engines, J. Non-Equilib Thermodyn **39**, 199 (2014).
[3] M. Santillán, G. Maya, and F. Angulo-Brown, J. Phys. D **34**, 2068 (2001).
[4] L. Guzmán-Vargas, I. Reyes-Ramírez, and N. Sánchez, J. Phys. D **38**, 1282 (2005).
[5] J. Chimal-Eguia, L. Guzmán-Vargas, and I. Reyes-Ramírez, Open Syst. Info. Dyn. **14**, 411 (2007).
[6] Y. Huang, D. Sun, and Y. Kang, Appl. Thermal. Eng. **29**, 358 (2009).
[7] D. Ladino-Luna, P. Portillo-Díaz, and R. T. Páez-Hernández, J. Mod. Phys. **4**, 22 (2013).
[8] L. Chen, X. Wu, Q. Xiao, Y. Ge, and F. Sun, Eniron. Eng. Manage. J. **14** (2015).
[9] M. Barranco-Jiménez, N. Sánchez-Salas, and F. Angulo-Brown, Entropy **13**, 171 (2011).
[10] M. Barranco-Jiménez, N. Sánchez-Salas, and M. Rosales, Entropy **11**, 443 (2009).
[11] M. Barranco-Jiménez, N. Sánchez-Salas, and I. Reyes-Ramírez, Entropy **17**, 8019 (2015).
[12] Y. Huang, D. Sun, and Y. Kang, J. Appl. Phys. **102**, 034905 (2007).
[13] Y. Huang and D. Sun, j. Nonequilib. Thermodyn. **33**, 61 (2008).
[14] Y. Huang and D. Sun, Int. J. Refrig. **31**, 483 (2008).
[15] Y. Huang and D. Sun, Appl. Therm. Eng. **28**, 1443 (2008).
[16] W. Nie, J. He, B. Yang, and X. Qian, Appl. Therm. Eng. **28**, 699 (2008).
[17] W. Nie, J. He, and X. Deng, Int. J. Therm. Sci. **47**, 633 (2008).
[18] Y. Huang, Energy Convers. Manag. **50**, 1444 (2009).
[19] J. He, G. Miao, and W. Nie, Phys. Scr. **82**, 025002 (2010).
[20] X. Wu, L. Chen, Y. Ge, and F. Sun, Appl. Math. Model. **39**, 1689 (2015).
[21] P. A. N. Wouagfack, G. F. Keune, and R. Tchinda, Int. J. Refrig. **75**, 38 (2017).
[22] I. Reyes-Ramírez, M. Barranco-Jiménez, A. Rojas-Pacheco, and L. Guzmán-Vargas, Entropy **16**, 5796 (2014).
[23] I. Reyes-Ramírez, M. Barranco-Jiménez, A. Rojas-Pacheco, and L. Guzmán-Vargas, Physica A **399**, 98 (2014).
[24] M. Esposito, R. Kawai, K. Lindenberg, and C. Van den Broeck, Phys. Rev. Lett. **105**, 150603 (2010).
[25] C. de Tomás, A. C. Hernández, and J. M. M. Roco, Phys. Rev. E **85**, 010104(R) (2012).
[26] Y. Wang, M. Li, Z. C. Tu, A. C. Hernández, and J. M. M. Roco, Phys. Rev. E **86**, 011127 (2012).
[27] Y. Hu, F. Wu, Y. Ma, J. He, J. Wang, A. C. Hernández, and J. M. M. Roco, Phys. Rev. E **88**, 062115 (2013).
[28] T. Schmiedl and U. Seifert, Europhys. Lett. **81**, 20003 (2008).
[29] Y. Izumida and K. Okuda, Europhys. Lett. **97**, 10004 (2012).
[30] M. Reséndiz-Antonio and M. Santillán, Physica A **409**, 162 (2014).
[31] J. Gonzalez-Ayala, A. Calvo Hernández, and J. M. M. Roco, Phys. Rev. E **95**, 022131 (2017).
[32] S. H. Strogatz, *Nonlinear Dynamics and Chaos: With Applications to Physics, Biology, Chemistry, and Engineering* (Westview Press, Boulder, 2014).

[33] A. Calvo Hernández, A. Medina, and J. M. M. Roco, New J. Phys. **17**, 075011 (2015).
[34] J. Gonzalez-Ayala, A. Calvo Hernández, and J. M. M. Roco, J. Stat. Mech. (2016) 073202.
[35] V. Holubec, J. Stat. Mech. (2014) P05022.
[36] V. Holubec and A. Ryabov, Phys. Rev. E **92**, 052125 (2015).
[37] P. R. Zulkowski and M. R. DeWeese, Phys. Rev. E **92**, 032113 (2015).
[38] R. S. Whitney, Phys. Rev. Lett. **112**, 130601 (2014).
[39] R. S. Whitney, Phys. Rev. B **91**, 115425 (2015).
[40] A. Ryabov and V. Holubec, Phys. Rev. E **93**, 050101 (2016).
[41] V. Holubec and A. Ryabov, J. Stat. Mech (2016) 073204.
[42] R. Long and W. Liu, Phys. Rev. E **94**, 052114 (2016).
[43] A. Dechant, N. Kiesel, and E. Lutz, arXiv:1602.00392v1.